Lukas C. van Dijk, MD
Jacqueline van Holten, MD
Bastiaan P. van Dijk, BSc
Niels A. A. Matheijssen, PhD
Peter M. T. Pattynama, MD

Index terms:
Magnetic resonance (MR), artifact, 9∗.129412, 9∗.12942[2]
Magnetic resonance (MR), vascular studies, 9∗.129412, 9∗.12942
Stents and prostheses, 9∗.1268

Radiology 2001; 219:284–287

[1] From the Department of Radiology, Erasmus University Medical Center Rotterdam, "Dijkzigt," Dr Molewaterplein 40, 3015 GD Rotterdam, the Netherlands (L.C.v.D., J.v.H., N.A.A.M., P.M.T.P.), and Elephant Dental, Hoorn, the Netherlands (B.P.v.D.). Received March 7, 2000; revision requested April 26; revision received August 1; accepted September 6. **Address correspondence to** L.C.v.D. (e-mail: *lcvandijk@rond.azr.nl*).

B.P.v.D. is a research and development employer for Elephant Dental.

[2] 9∗. Vascular system, location unspecified

Author contributions:
Guarantors of integrity of entire study, L.C.v.D., P.M.T.P.; study concepts, all authors; study design, L.C.v.D., J.v.H., N.A.A.M.; literature research, L.C.v.D., J.v.H.; experimental studies, L.C.v.D., J.v.H., B.P.v.D., N.A.A.M.; data acquisition, L.C.v.D., J.v.H.; data analysis, all authors; manuscript preparation, L.C.v.D., J.v.H.; manuscript editing, B.P.v.D., N.A.A.M., P.M.T.P.; manuscript review, N.A.A.M., P.M.T.P; manuscript final version approval, all authors.

A Precious Metal Alloy for Construction of MR Imaging–compatible Balloon-expandable Vascular Stents[1]

The authors developed ABI alloy, which mechanically resembles stainless steel 316. The main elements of ABI alloy are palladium and silver. Magnetic resonance (MR) images and radiographs of ABI alloy and stainless steel 316 stent models and of nitinol, tantalum, and Elgiloy stents were compared. ABI alloy showed the least MR imaging artifacts and was more radiopaque than stainless steel 316. ABI alloy has the potential to replace stainless steel 316 for construction of balloon-expandable MR imaging–compatible stents.

Magnetic resonance (MR) angiography is gaining importance as a vascular imaging modality (1) and has the potential to replace digital subtraction angiography for the detection of recurrent stenosis after stent placement in peripheral and coronary arteries. Metal stents implanted in the body, especially those made of stainless steel 316, cause major MR imaging artifacts, which are known as black-hole artifacts (2). Therefore, MR angiography provides no information about vessel segments that have stents or vessel areas that are close to the metal stent. Almost all stents placed in the coronary system and about half of those placed in the peripheral system are balloon-expandable devices made of stainless steel 316. Thus, to improve the reliability of MR imaging after balloon-expandable stent placement, a stent material with better MR imaging compatibility than stainless steel 316 is needed.

The MR imaging compatibility of a metal alloy depends on the type and quantity of elements used. Iron-containing alloys in particular and, to a lesser extent, alloys that contain cobalt, nickel, or chromium are known to cause MR imaging artifacts (3) and therefore degrade the MR imaging characteristics of vascular stents. We developed ABI alloy, a metal alloy composed of precious metal elements. The purpose of this initial study was to test the MR imaging compatibility of stents made of ABI alloy, especially as compared with those made of stainless steel 316. Because it is known that some MR compatibility is achieved with the use of other metal alloys, such as nitinol (4–6) and tantalum (7), we also compared the MR imaging of ABI alloy with that of commercially available stents made of nitinol, tantalum, and Elgiloy (Elgiloy, Elgin, Ill).

Materials and Methods

ABI alloy is an iron- and nickel-free precious metal alloy. The two main elements of this alloy are palladium and silver. The mechanical properties of ABI alloy have been tested by using industrial examinations. The elasticity was 1.1×10^5 N/mm^2; the elongation, 30%; and the hardness, 220 Hv (International Standards Organization no. 6892). These values are in the same range as those for stainless steel 316. The biocompatibility of this precious metal alloy group has been proved in industrial tests conducted by North American Science Associates, including tests for genotoxicity, cytotoxicity, local effects after implantation, irritation and sensitization, and hemolysis (International Standards Organization nos. 10993-3, 10993-5, 10993-6, 10993-10, and MG074-100, respectively; North American Science Associates, Northwood, Ohio).

We performed three MR imaging examinations. In the first examination, a self-made stent model made of stainless steel 316 was compared with an identical stent model made of ABI alloy. Both models were composed of two 0.4-mm-

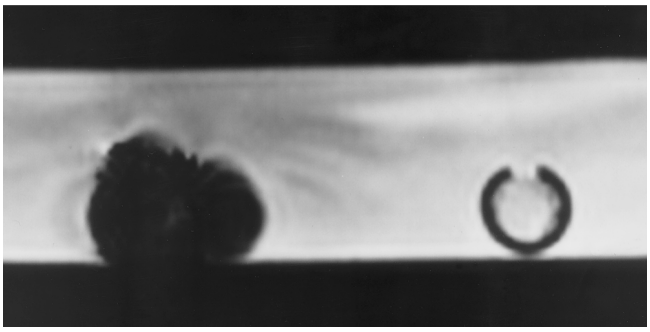

Figure 1. Transverse gradient-echo MR image (10.0/6.2) of stainless steel 316 (left) and ABI alloy (right) stent models. Right: The stent struts (gray area), stent lumen (white area), and plastic tube (black outer circle with gap at the top, which corresponds to a hole that allows air bubbles to escape) can be differentiated. The stainless steel stent, stent lumen, and plastic tube surrounding the stent cannot be differentiated.

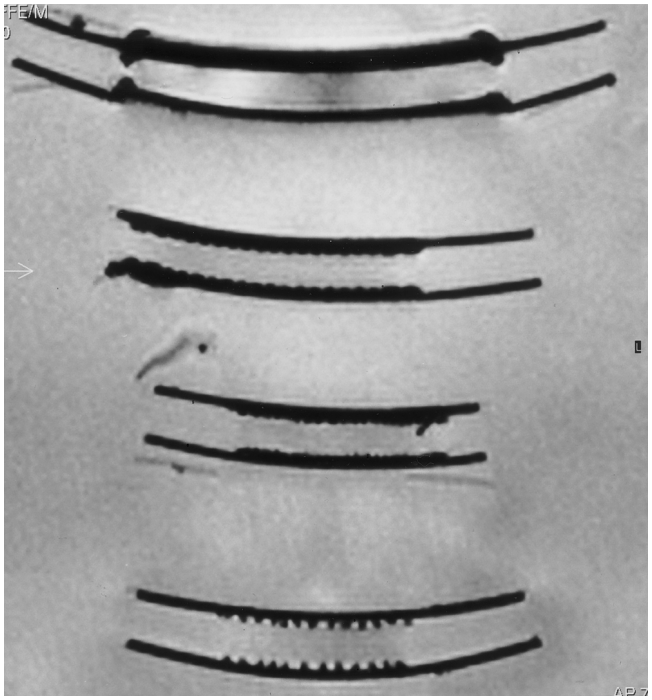

Figure 2. Coronal gradient-echo MR image (10.0/6.2) of, from top to bottom, the Elgiloy, nitinol, and tantalum stents and the ABI alloy stent model. The plastic tubes in which the stents are mounted show no signal intensity. The artifacts of the stents within the tubes caused a virtual lumen reduction in the Elgiloy (30%), nitinol (20%), and tantalum (20%) stents. The struts of the ABI alloy stent model are visible as black dots.

Semiquantitative Description of Stent Artifacts

Device	Artifact
Test 1	
Self-made ABI-alloy stent model, 0.4 mm-wire	+
Self-made stainless-steel stent model, 0.4-mm wire	++++
Test 2	
Elgiloy stent	+++
Nitinol stent	++
Tantalum stent	++
Self-made ABI-alloy stent model, 0.4-mm wire	+

Note. —+ = mild artifact, ++ = moderate artifact, +++ = severe black-hole artifact, ++++ = severe black-hole artifact with marked image distortion.

thick wires made into a helix—one clockwise and the other counterclockwise. The two wires were bound together by using silk at each wire crossing to form a basic expanded stent model with a length of 40 mm, diameter of 8 mm, and 12 loops.

In the second examination, we compared the self-made ABI alloy stent model with the following commercially available devices: Memotherm nitinol stent (Bard Interventional Products, Billerica, Mass), Strecker tantalum stent (Boston Scientific/Vascular, Watertown, Mass), and Wallstent elgiloy stent (Schneider, Minneapolis, Minn), all of which have a diameter of 8 mm.

In the third examination, the ABI alloy stent model was compared with the nitinol stent by using a three-dimensional volume gradient sequence, because it is known that nitinol stents have the best MR imaging compatibility.

The MR imaging experiments were carried out with a 1.5-T magnet (ACS-NT; Philips Medical Systems, Best, the Netherlands) and a surface coil. In the first two examinations, images were obtained with a gradient-echo technique (10.0/6.2 [repetition time msec/echo time msec], 30° flip angle, 205 × 256 matrix, 2-mm section thickness). In the third examination, a three-dimensional gradient-echo technique was used (27.0/7.3, 30° flip angle, 512 × 512 matrix, 0.8-mm section thickness). The devices were placed in plastic tubing that was taped to the bottom of a plastic container. The tube and the container were filled with a copper sulfate in water solution (1 g/L).

The presence and degree of artifacts on the resulting MR images were quantified according to the method of Teitelbaum et al (8): no artifact, mild artifact, moderate artifact, severe black-hole artifact, and severe black-hole artifact with marked image distortion (Table). A mild artifact was judged to be smaller than the device causing the artifact (8). A moderate artifact was approximately the same size as the device. A severe black-hole artifact was larger than the device. Distortion was defined as bending, warping, or obliteration of the image contours normally observed.

The virtual lumen reduction caused by the MR artifacts was estimated, in steps of 10%, after measuring the luminal diameter of the stents and of the tubes surrounding the stents on the MR images (Figs 1, 2).

In addition to MR imaging, we used a differential method to determine the radiopacity of stainless steel 316 and ABI alloy (9). Simultaneously to imaging the stent models, a radiograph of an aluminum wedge was obtained at 60 kV and with 25-mm aluminum filtering. A comparison was made on the radiograph between the optical density (ie, blackening) produced by the wedge and the points of interest of the two stent models. The aluminum thickness values of the wedge, which produced the same optical density as the stent models on the radiograph, were read. The optical densities of the stent model materials were expressed in millimeters of aluminum equivalent.

Results

The measurements of the MR imaging artifacts caused by the different materials

are summarized in the Table. In test 1, the stainless steel 316 model caused severe black-hole artifacts with marked distortion of the MR images. The ABI alloy model caused mild artifacts that were smaller than the stent model device (Fig 1).

In test 2, the Elgiloy stent caused a severe black-hole artifact, the nitinol and tantalum stents caused moderate artifacts, and the ABI alloy stent model caused a mild artifact (Fig 2).

In test 3, the ABI alloy stent model caused fewer artifacts than did the nitinol stent (Fig 3). On the MR images of the ABI alloy stent model, delineation of the plastic tube from the stent material was possible, but this was not the case with the nitinol stent. Both the nitinol stent and the ABI alloy stent model caused some signal intensity decrease within the lumen.

The virtual lumen reduction caused by the MR artifacts was 0% (lumen, 10 mm; tube, 10 mm) for the ABI alloy model, 100% (lumen, 0 mm; tube, 10 mm) for the stainless steel 316 model, 20% (lumen, 8 mm; tube, 10 mm) for the nitinol stent, 20% (lumen, 8 mm; tube, 10 mm) for the tantalum stent, and 30% (lumen, 8 mm; tube, 11 mm) for the Elgiloy stent (Figs 1, 2).

With use of the differential method to determine the radiopacity of both metal alloys, stainless steel 316 was equal to a 5.4-mm aluminum equivalent (±0.5 mm) and ABI alloy was equal to a 12.8-mm aluminum equivalent (±0.5 mm). ABI alloy was therefore approximately 2.4 times more radiopaque than stainless steel 316 (Fig 4).

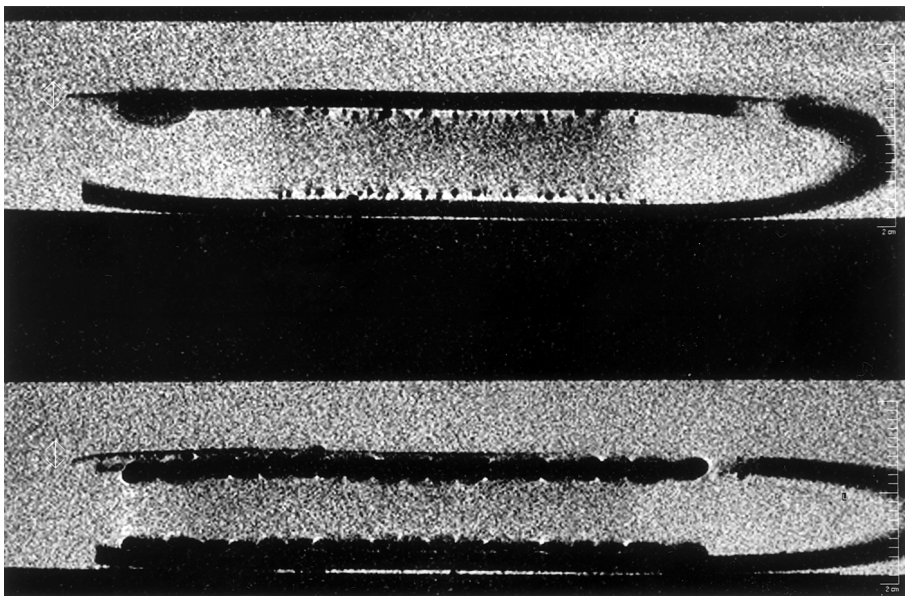

Figure 3. Sagittal gradient-echo MR image (27.0/7.3) of the ABI alloy stent model (top) and the nitinol stent (bottom). The plastic tubes show no signal intensity. The ABI alloy stent model shows no virtual lumen reduction; the stent material can be recognized by the black dots. The nitinol stent caused moderate artifacts that resulted in a virtual lumen reduction on the image.

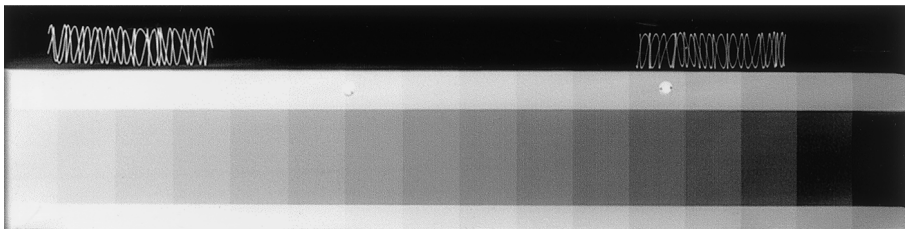

Figure 4. Radiograph (60 kV, 25-mm aluminum filtering) of the aluminum wedge (bottom) and the ABI alloy (left) and stainless steel 316 (right) stent models. ABI alloy was approximately 2.4 times more radiopaque than stainless steel 316.

Discussion

The results of this in vitro study show that ABI alloy causes substantially fewer artifacts at MR imaging than does stainless steel 316.

Balloon-expandable stents are preferred for the coronary arteries by almost all interventional cardiologists and for several peripheral vessels by many interventional radiologists because of their accuracy and ease of placement compared with those of self-expandable stents. Stainless steel 316 has the mechanical properties necessary for construction of balloon-expandable stents—that is, plastic deformability to allow crimping on a low-profile balloon and expansion to the vessel diameter, combined with good hoop strength at full expansion and resistance to breakage. Because the mechanical properties of ABI alloy are similar to those of stainless steel 316, our main goal was to compare this material with the standard materials used to construct balloon-expandable stents.

Artifacts in stents on MR images are dependent on the material and design of the stents. In the first test, we used self-made stent models with an identical design, which allowed a comparison of the (isolated) effect of the different materials. In the second test, the stent materials and stent designs were different. Therefore, the different MR artifacts observed with the ABI alloy stent model and the nitinol, tantalum, and Elgiloy stents were caused by a combination of material and design influences. Because stent design is dictated by many factors, including the mechanical properties of the material and patent issues, to our knowledge clinically tested stents of identical design but different material are not yet available for in vitro and in vivo comparisons of MR artifacts.

MR artifacts are dependent on the MR sequence. In the described experiments, we used gradient-echo sequences with relatively long echo times to exaggerate the artifact sizes, because longer echo times are associated with larger artifacts. Modern MR systems allow fast imaging sequences for MR angiography and coronary MR angiography with shorter repetition and echo times. It is reasonable to assume that the severity of artifacts will be reduced if these sequences are used, but the differences between the materials will still exist.

MR evaluation of the stent lumen is, to some extent, possible with nitinol and tantalum stents (5,10), but only stenoses of 50% or more can be correctly assessed, because smaller stenoses are overestimated owing to the artifacts (11). The ABI alloy stent model allowed clear delineation of the stent from the plastic tube

surrounding the stent. This suggests that with ABI alloy stents, not only MR imaging evaluation of stent patency but also MR analysis of the vessel wall surrounding the stent is possible. The ability to image close to the stent material could mean that MR angiographic evaluation of even mild within-stent recurrent stenosis is possible after ABI alloy stent placement. In the lumina of both the ABI alloy stent model and nitinol stent, some MR signal intensity decrease was noticeable, probably owing to the Faraday cage effect.

The radiograph showed that the radiopacity of ABI alloy is approximately 2.4 times higher than that of stainless steel 316. This implies that fluoroscopic imaging for positioning of stents made of ABI alloy should be at least as good as that for positioning of stents made of stainless steel 316 when stents of identical design are compared. In conclusion, initial examination results showed that ABI alloy causes fewer artifacts at MR imaging than does stainless steel 316.

References

1. Duerinckx AJ. Coronary MR angiography. Radiol Clin North Am 1999; 37:273–318.
2. Bernardino ME, Steinberg HV, Pearson TC, Gedaudas-McClees RK, Torres WE, Henderson JM. Shunts for portal hypertension: MR and angiography for determination of patency. Radiology 1986; 158:57–61.
3. Bellon EM, Haacke EM, Coleman PE, Sacco DC, Steiger DA, Gangarosa RE. MR artifacts: a review. AJR Am J Roentgenol 1986; 147:1271–1281.
4. Nitatori T, Hanaoka H, Hachiya J, Yokoyama K. MRI artifacts of metallic stents derived from imaging sequencing and the ferromagnetic nature of materials. Radiat Med 1999; 17:329–334.
5. Hilfiker PR, Quick HH, Debatin JF. Plain and covered stent-grafts: in vitro evaluation of characteristics at three-dimensional MR angiography. Radiology 1999; 211:693–697.
6. Schurmann K, Vorwerk D, Bucker A, et al. Perigraft inflammation due to Dacron-covered stent-grafts in sheep iliac arteries: correlation of MR imaging and histopathologic findings. Radiology 1997; 204:757–763.
7. Amano Y, Gemma K, Kawamata H, Kumazaki T. Intraluminal signal intensity of iliac artery stents investigated by contrast-enhanced three-dimensional MR angiography. Comput Med Imaging Graph 1998; 22:9–12.
8. Teitelbaum GP, Bradley WG, Klein BD. MR imaging artifacts, ferromagnetism, and magnetic torque of intravascular filters, stents, and coils. Radiology 1988; 166: 657–664.
9. Balz G, Birkner R. Die bestimmung des aluminiumschachungsgleichwertes von knochengewebe beim lebenden. Strahlentherapie 1956; 99:221–226.
10. Matsumoto AH, Teitelbaum GP, Carvlin MJ, Barth KH, Savin MA, Strecker EP. Gadolinium enhanced MR imaging of vascular stents. J Comput Assist Tomogr 1990; 14:357–361.
11. Link J, Steffens JC, Brossmann J, Graessner J, Hackethal S, Heller M. Iliofemoral arterial occlusive disease: contrast-enhanced MR angiography for preinterventional evaluation and follow-up after stent placement. Radiology 1999; 212:371–377.